Pediatric and adult-onset HCM mutations in the myosin motor domain have similar properties

Carlos D Vera[1,#], Chloe A Johnson[2,#], Jonathan Walklate[2], Arjun Adhikari[3], Zoltan Ujfalusi[4], Marina Svicevic[5], Srba M Mijailovich[6], Ariana Combs[1], Stephen J. Langer[1], Kathleen M. Ruppel[7], James A. Spudich[7], Leslie A. Leinwand[1,*], and Michael A. Geeves[2,*]

From the [1]BioFrontiers Institute and Department of Molecular, Cellular and Developmental Biology, University of Colorado Boulder, Boulder CO 80309 USA; [2]School of Biosciences, University of Kent, Canterbury UK, CT2 7NJ; [3]Rumi Scientific, San Francisco CA 94107 USA; [4]Department of Biophysics, University of Pécs, Medical School, Szigeti Street 12, H-7624 Pécs, Hungary, [5]Faculty of Science, University of Kagujevac, Serbia; [6]Department of Biology, Illinois Institute of Technology, Chicago IL 60616 USA; [7]Stanford University School of Medicine, Department of Biochemistry, Stanford CA 94305 USA.

Running title:

*To whom correspondence should be addressed: Michael A. Geeves School of Biosciences, University of Kent, Canterbury, UK, CT2 7NJ m.a.geeves@kent.ac.uk; Leslie A. Leinwand BioFrontiers Institute and/or Department of Molecular, Cellular and Developmental Biology, University of Colorado, Boulder CO 80309 leslie.leinwand@colorado.edu

[#]CDV & CAJ contributed equally to this work

Key words: Human cardiomyopathies, hypertrophic cardiomyopathies, dilated cardiomyopathies, acto-myosin kinetics, kinetic modeling

Abstract

Hypertrophic Cardiomyopathy (HCM) is a common genetic disorder that typically involves left ventricular hypertrophy and abnormal cardiac contractility. Mutations in *β-MyHC* are a major cause of HCM and are typically characterized with cardiac hypercontractility, but the specific mechanistic changes to myosin function that lead to the disease remain incompletely understood. Predicting the severity of any single *β-MyHC* mutation is hindered by a lack of detailed evaluation at the molecular level. In addition, since the cardiomyopathy can take 20 - 40 years to develop, the severity of the mutations must be somewhat subtle. We hypothesized that mutations which result in childhood cardiomyopathies may show a more severe indication of molecular changes in myosin and be therefore easier to identify. In this work, we performed steady-state and transient kinetics analysis of the myosin carrying one of eight miss sense mutations in the motor domain. Five of these have been identified in childhood cardiomyopathies. The derived parameters were used to model the ATP driven cross bridge. Contrary to our hypothesis, the results show no clear differences between early and late onset HCM mutations. Despite the lack of distinction between early and late onset HCM, the predicted A·M·D occupancy for [A] = 3 K_{app} along with the closely related Duty Ratio (*DR*) and the measured ATPases all change in parallel (in both sign and degree of change) compared to the WT values. Six of the eight HCM mutations are clearly distinct from a set of DCM mutations previously characterized.

The most common inherited cardiomyopathy is Hypertrophic CardioMyopathy (HCM) with a disease-prevalence of 1:250-500 (Harris et al., 2006; Hershberger, Hedges, & Morales, 2013). Excluding those with a history of hypertension, aortic stenosis, other pre-existing systemic diseases, or being a world-class athlete, HCM is diagnosed as unexplained left ventricular hypertrophy and is typically accompanied by diastolic dysfunction (Stewart, Mason, & Braunwald, 1968). The first mutated gene causing HCM, *MYH7* or β-cardiac myosin heavy chain, was reported almost 30 years ago (Geisterfer-Lowrance et al., 1990; Jarcho et al., 1989). There are now thousands of mutations in proteins of the sarcomere that account for 60-70% of HCM cases (Teekakirikul, Kelly, Rehm, Lakdawala, & Funke, 2013). There are eight major sarcomeric proteins that are implicated in the majority of HCM index cases and their families, with 60-70% found in either β-cardiac myosin or myosin-binding-protein C (*MyBPC*). This suggests that myosin is an important target for therapeutic intervention (Ashrafian, McKenna, & Watkins, 2011; Green et al., 2016).

We consider here the difference between myosin mutations causing early-onset versus adult-onset HCM. We hypothesized that β myosin mutations associated with early-onset HCM would be more severe than those mutations seen in individuals who are diagnosed later in life. Analysis of the biochemical and biophysical properties of these 2 classes of myosin's should reveal the severity of the mutational changes. We compared the properties of known adult pathogenic mutations (R719W, R723G, & G741R) with novel sporadic mutations that had appeared in recent cardiomyopathy screens as unique to pediatric patients (H251N, D382Y, F540L, P710R and V763M) (Cuenca et al., 2016; Kaski et al., 2009a; Morita et al., 2008). We produced recombinant mutant and wild type

human myosin motors in differentiated C2C12 muscle cells, performed extensive kinetic analysis, and evaluated the severity of these mutations based on alterations to the cross-bridge cycle.

The location of eight residues in the *MYH7* gene under consideration here is shown in Fig. 1A. The high degree of conversation underscores the importance of these sites (Fig. 1B). Myosin is very vulnerable to mutations and there are now >400 different mutations described in *MYH7* (Colegrave & Peckham, 2014; Hamady, Buvoli, Leinwand, & Knight, 2010). A number of disease-causing *MYH7* mutations have been studied in the context of recombinant human *β-MyHC* motors (Adhikari et al., 2016; Bloemink et al., 2014; Kawana, Sarkar, Sutton, Ruppel, & Spudich, 2016; Nag et al., 2015; Palmer et al., 2004; Seebohm et al., 2009; Sommese et al., 2013). R403Q, R453C, R719W, R723G, G741R, and D239N are mutations that are widely recognized as pathogenic and have been seen in multiple families (ClinVar). The pediatric H251N, D382Y, F540L, P710R, and V763M mutations are less prevalent and their pathogenicity has not yet been clearly established (ClinVar).

H251 is in the central β-sheet (Fig.1A) that undergoes strain-induced twisting upon ATP-binding and communicates to the 50K domain to open and release actin. H251N was identified in a screen of 79 preadolescent children and later characterized biophysically (Adhikari et al., 2016; Kaski et al., 2009a). Adhikari *et al* found that this early-onset mutation resulted in higher k_{cat}, actin-gliding velocity, and intrinsic force (Adhikari et al., 2016). Located close to the cardiomyopathy loop of the actin binding domain, D382Y has been categorized as a variant of unknown (or uncertain) significance (VUS) (Kaski et al., 2009, ClinVar). Close to this residue is the well-studied pathogenic R403Q

mutation which had subtle biophysical changes compared to WT (Nag et al., 2015). F540L is found on a helix-loop-helix motif on the lower 50kDa domain (L50) and was re-classified in recent years from VUS to pathogenic, and from Dilated CardioMyopathy (DCM) to HCM (Cuenca et al., 2016, ClinVar). On the L50 there is an α-helix that is a "hot spot" of cardiomyopathy-related mutations, namely: I524V, E525K, M531R, S532P, I533V, and our residue of interest, F540L (J. A. Spudich, 2015). M531R and S532P are mutants linked to Left Ventricular Non-Compaction (LVNC) and DCM respectively, and even though these residues are right next to each other, they displayed opposite biophysical properties (Aksel, ChoeYu, Sutton, Ruppel, & Spudich, 2015). P710, a residue on the border of the relay/converter junction site, has been reported to be mutated to an arginine or a histidine (Kaski et al., 2009a; Kindel et al., 2013). P710H is considered pathogenic, while P710R has been reported once, making it a rare mutation (Kaski et al., 2009a; Kindel et al., 2013).

The myosin converter is well-known to be enriched for HCM-causing mutations with a range of adverse effects (García-Giustiniani et al., 2015; Homburger et al., 2016). Converter mutations studied here include the adult onset mutations R719W, R723G, and G741R and the early-onset mutation V763M. Muscle biopsy and skinned fiber studies have shown the converter domain adult-onset mutations have increased fiber stiffness with subtle changes in cross-bridge kinetics analysis (Cuda, Fananapazir, Epstein, & Sellers, 1997; Fananapazir, Dalakast, Cyran, Cohn, & Epstein, 1993; Köhler et al., 2002; Lowey et al., 2008; Seebohm et al., 2009; Tyska et al., 2000). The steady-state k_{cat}, the actin gliding velocities, and intrinsic force measurements of the myosin motor domain for these adult-onset pathogenic HCM mutations did not vary much when compared to WT

(Kawana et al., 2016). Although V763M has been seen in multiple people and multiple families with HCM (Kaski et al., 2009b; Mohiddin et al., 2003), it is also classified as both an early-onset mutation and a VUS (ClinVar).

We previously performed kinetic analysis of five adult-onset DCM mutations in *β-MyHC* (Ujfalusi, 2018). Overall, our analysis did not reveal a pattern of common defects in individual steps of the cycle, other than a few altered properties specific to the myosin subdomain where the mutation is localized. However, a pattern did emerge when the full cycle was modeled using all the data from ATPase and stopped-flow experiments (Srbolujub M. Mijailovich et al., 2017). Modeling predicted that the DCM mutations altered the steady-state motor function and the state occupancies in the minimal 8-step cross-bridge cycle in a manner consistent with a loss of the ability to generate steady-state force (Ujfalusi et al. 2018). Here, for the early- and late-onset HCM mutations, we show that the kinetic parameters of mutations also do not have a "unifying" disruption of the cycle. However, the strongly attached actin-myosin states are significantly affected. Contrary to our hypothesis, we did not detect any strong differences between mutations seen in adult-onset versus early-onset patients, or among mutations in the different structural-domains of the motor.

Results

ATPases

Steady-state ATPase data for four of the mutations examined here have already been published these are listed in Table 1 together with the k_{cat} values for the remaining four mutations. The error on these measurements is of the order of 10% and three of the mutations differ from WT by less than 5%; the early onset D382Y, and V763M and the

adult G741R. Two mutations, early onset H251N and adult R719W differ from WT by 24 and 20% respectively which is significant while the remaining mutations, F540L, P710R and the adult R723G are more significant with 29-42% changes. Note that these five mutations show both increased and decreased k_{cat} values. There is thus no common pattern of change in the k_{cat} values for these HCM mutations and no difference in pattern between early and late onset groups. This lack of common patterns led us to focus on the transient kinetic analysis which can reveal more detail about how the mutations change the ATPase cycle.

Transient kinetics data summary

Considerable amounts of pre-steady state kinetic data have been collected for a number of DCM and HCM mutations in the *β-MyHC* motor domain. The descriptions of methods, analysis tools, model assumptions, data quality and details of the measurements have been set out in our earlier work (Bloemink et al., 2014; Deacon, Bloemink, Rezavandi, Geeves, & Leinwand, 2012; Srbolujub M. Mijailovich et al., 2017; Nag et al., 2015; Ujfalusi et al., 2018). We have taken the same approach to understand the impact of this set of HCM mutations and to compare to the results of previous studies. Details of individual measurements and the evaluation of data quality are presented in the Supplementary Information. Here we focus on what effect each mutation has on the behavior of the cycle. For every mutant, each measurement was made at least three times with a minimum of two independent protein preparations. In general, all parameters were measured to a precision of better than 20% and in most cases better than 10%. We assume any change of less than 20% is of little significance.

The data are interpreted in terms of the 8-step ATP driven cross bridge cycle that we have used previously (Fig. 2). Red shades indicate detached cross-bridges, yellow shades are weakly-attached, and blue shades represent strongly-attached force-holding cross bridges. Table 1 shows the mean values and errors of the actin and nucleotide binding experiments for the steps in the cycle that are accessible together with the ATPase parameters. There is a large amount of information in Table 1 and to make the overall pattern of the induced changes clearer, the percent changes relative to WT are color coded in the table. The data are also summarized in Fig. 3, where the percentage differences in each parameter relative to WT are plotted.

Interaction of myosin with nucleotide in the absence of actin

Even though the reactions are not part of the normal cycle, nucleotide binding to the motor in the absence of actin is measured to understand how the nucleotide binding pocket and the weakly-attached actin states might be affected by the mutations. The affinity of ATP for sS1 (short S1) is weakened >1.7-2-fold for two mutations (D382Y, P710R and G741R). All other mutations were 20-30% weaker except R719W which was indistinguishable from WT. In contrast, most mutants bound ADP >2-fold tighter, with the exception of R723G (just less than 2-fold tighter) and P710R (6-fold weaker). Thus, no simple pattern of behavior was apparent for the sS1 in the absence of actin.

Interaction of sS1 with nucleotide in the presence of actin

The darker color coding of the data in Table 1 shows the parameters that change >2-fold (dark blue decrease, dark orange increase) and indicate that a large number of parameters have been affected. Thus the changes observed are not minor, despite relatively small changes in the value of the steady-state k_{cat}.

Fig. 3A shows that in general, the value of $1/K_T$ (the affinity of ATP for acto.sS1) K_A and K_{DA} (the affinity of actin for sS1 and sS1.ADP) has tighter binding (decrease in measured parameter) of > 20%, but none is as much as 2-fold tighter. Within each set of measurements there are exceptions ($1/K_T$ for F540L, K_A for R723G), but there is a pattern. In contrast, the affinity of ADP for acto.sS1 is >2-fold weaker in five cases, while F540L and R723G are not significantly different from WT.

Fig. 3B shows changes in measured rate constants and there is some consistent behavior but not uniform for all mutations. The maximum rate constant for sS1 detachment from actin upon binding ATP (k_{+T}) is generally slower (20-70%) with the exception of F540L which is increased by 30%), and the rate constant for of ADP binding to acto.S1 is also generally slower (30-70%) with the exception of R723G which is increased by 70%. All other rate constants had variable changes or none at all. This highly variable pattern was also seen for the set of DCM mutations we previously reported (Ujfalusi et al., 2018).

Modeling the ATPase cycle of HCM mutant motors

We modeled the complete cycle using all of our kinetic data following the approach outlined in recent papers comparing different myosin isoforms and different DCM-causing mutations in *MYH7* (Srbolujub M. Mijailovich et al., 2017; Ujfalusi et al., 2018). The transient kinetics data provides definition for six of the eight steps of the cycle with a precision generally of ±20%. When combined with ATPase data (k_{cat} and K_{app}), the full cycle allows us to predict acto·myosin occupancy of states (Fig. 4; Supp. Table 3), along with key properties of the cycle: duty ratio, shortening velocity, steady-state force (Fig. 5; Supp. Table 2), and ATP-economy (Fig. 7). Under isometric conditions in a muscle fiber,

because of the mismatch of the thick and thin filament helicity, some myosin heads have readily accessible actin while others do not. We therefore modeled a range of actin concentrations ([A] = K_{app}, *3* K_{app}, and *20* K_{app}, where the ATPase rate is 50, 75, and 98% of k_{cat} values, respectively) to facilitate comparison between the different mutant constructs under conditions that may match those of a contracting sarcomere. In addition, we modeled contraction under load as previously, by assuming both ADP and P_i release steps were inhibited 3-fold under a 5-pN load for all mutations (see *Discussion*).

The predicted occupancies are shown in Fig. 4. Note that the color schemes are the same in both Fig. 2 and Fig. 4; red shades indicate detached cross-bridges, yellow shades are weakly-attached, and blue shades represent strongly-attached force-holding cross bridges. The numbers by each pie chart represent the percentage of the pale blue, force-holding A·M·D state. The WT data predict at low actin concentration (*[A]* = K_{app}), almost 75% of cross-bridges are detached with just 5.2% in the force-holding blue states, dominated by the A·M·D state. As actin concentration increases, the detached-states (red) decrease, the weakly-attached states (yellow) increase, and the strongly-attached A·M·D state increases to 9.8% at 20 K_{app} increases. The application of a 5-pN load at *[A]* = *3* K_{app} increased the A·M·D state from 7.7 to 8.4% and increased the weakly-attached states (mainly A-M·D·P) at the expense of the detached M·T state. Note the occupancy values here are slightly lower than in (Ujfalusi *et al* 2018) because of a slightly lower WT k_{cat} value used within this consistent data set.

.

Examining pie charts in Fig. 4 for the mutations shows that the general distribution of states is very similar between WT and H251N although the force-holding A·M·D state was higher (~25%) for H251N at all actin concentrations. Similarly, the distribution was similar for D382Y, V763M, R719W and G741R, but the force-holding A·M·D states were marginally smaller (by about 10%) while the detached M·T states (deep red) were larger. For F540L, the A·M·D state occupancies are significantly larger and much smaller for P710R and R723G, respectively, compared to WT. These comparisons are easier to assess in Fig. 5 where the predicted A·M·D occupancy for [A] = 3 K_{app} with and without load are plotted along with the closely related Duty Ratio (*DR*) and the measured ATPases. All three parameters change in parallel (in both sign and degree of change) compared to the WT values.

The predicted velocity of shortening was estimated from the equation $V_o = d \cdot ATPase/DR$, where *d* is the step size (assumed to be invariant at 5 nm) and show little variation amongst the eight mutants. Only R719W and R723G are predicted to increase by more than 10% (Fig. 5). *In vitro* motility measurements have been published for several HCM mutations (Adhikari et al., 2016; Kawana et al., 2016). Unpublished data have been collected for the other HCM mutations studied here to consolidate with the kinetics data (Fig. 6) Fig. 6 shows the mean velocity of the top 5% of smoothly moving filaments, normalized to the WT values, compared with our predictions. The normalization to the WT values allows comparison between the two data sets despite the different constructs and different experimental conditions used. For five of the eight mutations, the predicted velocities are in good agreement with those measured. For the other three, there are large discrepancies. Our predictions were for little change in velocity for all mutations but

H251N and F540L; both of which moved much faster than WT while P710R was much slower than WT. We consider this discrepancy in the *Discussion*.

The modeling data also allow an estimate of the economy of ATP usage, another parameter that could be involved in the development of HCM (Neubauer, 2007) if it results in a metabolic imbalance in the muscle. The predicted rates of ATP usage are shown in Fig. 7 for both a muscle fiber holding a 5 pN load (ATP used per pN) and when shortening at the maximum velocity and when ATP is being turned over at k_{cat} (ATP/sec per μm moved). Once more, the changes in economy for each mutation, under both conditions reflected the changes in the ATPase rates relative to WT.

Discussion

We have presented here a detailed evaluation of the human β myosin motor domain carrying eight different HCM missense mutations. Before considering the implications of our data it is pertinent to point out the precision with which we can evaluate the data. All measured constants are defined to within an error of at least 20%, and in many cases better than 10%, using independent preparations of protein. The fitting of the data to the model uses all of the data to define the five missing constant in the 8-state cross bridge cycle (Fig. 2). In our previous studies of DCM mutations (Ujfalusi et al., 2018) and the α & β cardiac isoforms (Mijailovich et al., 2017) we showed the fitting was quite robust and that a ±20% change in any of the constants had minimal effect of the overall balance of the cycle except for the intermediate most directly affected by the varied constant. A similar analysis was carried out here (Supp. Table S5) so we are confident in the analysis of the cross bridge cycles presented.

Of the eight mutations studied, five have been identified in children with HCM and three have only been reported in adults with HCM (Supp. Table S1). We previously reported a similar characterization of two additional adult onset mutations, R403Q and R453C (Bloemink et al., 2014; Nag et al., 2015; Ujfalusi et al., 2018). The majority of mutations in myosin have been identified in adults and despite the mutant myosin's being present in the heart since birth, the cardiomyopathy can take 20-40 years to develop. We reasoned that early onset mutations may show more substantive changes in biophysical properties since they manifest earlier in life. The data presented here *do not* support this hypothesis. Each of the mutations (early-onset and adult-onset) exhibited a set of changes in the measured parameters by as much as 2-fold. However, no general pattern of change was apparent that identified either the early onset group or the group as a whole. This remained true when the data were used to model the cross bridge cycle (Figs. 4, 5, 7 Supp. Tables S2-4)

. We previously identified common traits amongst myosin's carrying one of five mutations associated with DCM (Ujfalusi et al., 2018). Most of the mutations were found to have a reduced k_{cat} lower occupancy of the force holding AMD state, a lower *DR,* and these myosins were more economical in the use of ATP for both rapid movement and force generation. Collectively, the myosin's had an impaired capacity to generate or maintain force when working as an ensemble. Curiously, two of the mutations examined here share these properties; the early onset P710R and the adult R723G, suggesting some overlap between the groupings.

The remaining six mutations show mostly modest changes in properties as was previously observed for the R403Q and R453C HCM mutations. The $k_{cat,}$ economy of

ATP usage and *DR*'s were similar to WT for D382Y, V763M, R719W and G741R while all three parameters were increased for H251N and F540L. Thus, for six of the eight HCM mutations the distinctions between HCM & DCM mutations that we previously reported remain valid. Although how the HCM mutations lead to the cardiomyopathy, remains to be defined.

The question of what distinguishes mutations associated with early onset of the myopathy remains a valid question but we need to address if the diagnosis of early onset is a distinct group. As shown in Table S1 each of these mutations, with the exception of F540L, has only been identified in a single patient with no other member of the family affected. Interestingly, F540L has been found to segregate in a family with DCM. It may be that factors in addition to the myosin mutation contribute to the disease. Alternatively, the assays performed here are purely *in vitro* with single motor domains and the mutant myosin's may need a cellular or tissue environment to manifest the full pathological consequences.

There is considerable interest in the role of the interactions between the two motors of myosin in forming a down-regulated form of the myosin the Interacting head motif, IHM (Alamo et al., 2017). Such motors are likely to be further stabilized by interactions with both the backbone of the thick filament and *MyBPC* (Alamo et al., 2017). Myosin mutations that destabilize the off-state would make more heads available and lead to a hyper-contractile state, thought by many to be the precursor to HCM (Alamo et al., 2017; Trivedi, Adhikari, Sarkar, Ruppel, & Spudich, 2017). The interaction between the off and on state of myosin is postulated to be regulated by phosphorylation of the *RLC*, or the *MyBPC*, mechanical strain on the thick filament, and possibly calcium (Linari et al., 2015;

Mohamed, Dignam, & Schlender, 1998; Previs et al., 2016; Toepfer et al., 2013) Destabilization of the off-state could occur by reducing motor-motor, motor-backbone or motor-MyBPC interactions. Any effect on the interacting heads could override the modest affects we report here, on the cross bridge cycle for most of the HCM mutations. This seems less likely to be the case for the two mutations that appear similar to the DCM mutations where the large reduction in k_{cat} (30-40%) and *DR* (40-50%) will have a significant effect on the working cardiac muscle. Any effect on the interacting heads would need to be very large to over-compensate for the loss of force-holding cross bridges in the steady-state caused by these changes in the duty ratio.

A recent study used the latest crystal structures docked into the lower resolution EM images of the interacting motors to identify regions of the motor directly involved with the interaction. This work was combined with a molecular dynamics study of 178 HCM mutations to suggest how mutations might affect myosin function (Robert-Paganin, Auguin, & Houdusse, 2018). HCM mutants were predicted to affect interacting heads, the stability of the M·D·P_i state required to form the interacting heads, the motor function or the stability of the motor or some combination of the effects. From the Robert-Paganin *et al* study our mutations H251N, R719W, R723G and G741R were predicted to affect motor function, and destabilize the sequestered state due to effects on IHM contacts, which is consistent with our results. P710R was predicted to alter motor function and destabilize the sequestered state by affecting the stability of the pre-power-stroke conformation, while V763M was predicted to affect mostly protein stability.

At the outset of this series of studies, we began with the expectation that there would be common molecular pathways for HCM vs DCM mutations. The work has defined

more sharply the types of things mutations can do to the myosin motor and still have a functioning heart. To understand the way in which the mutations lead to myopathies there is a need for more complex assays that include cells and/or engineered 3D tissues to integrate the signals in the muscle and converge to cause the disease. This includes the role of a heterozygous mixture of WT and mutant myosin's in tissue.

References

Adhikari, A. S., Kooiker, K. B., Sarkar, S. S., Liu, C., Bernstein, D., Spudich, J. A., & Ruppel, K. M. (2016). Early-Onset Hypertrophic Cardiomyopathy Mutations Significantly Increase the Velocity, Force, and Actin-Activated ATPase Activity of Human β-Cardiac Myosin. *Cell Reports*, *17*(11), 2857–2864. https://doi.org/10.1016/j.celrep.2016.11.040

Aksel, T., ChoeYu, E., Sutton, S., Ruppel, K. M., & Spudich, J. A. (2015). Ensemble Force Changes that Result from Human Cardiac Myosin Mutations and a Small-Molecule Effector. *Cell Reports*, *11*(6), 910–920. https://doi.org/10.1016/j.celrep.2015.04.006

Alamo, L., Ware, J. S., Pinto, A., Gillilan, R. E., Seidman, J. G., Seidman, C. E., & Padrón, R. (2017). Effects of myosin variants on interacting-heads motif explain distinct hypertrophic and dilated cardiomyopathy phenotypes. *ELife*, *6*, 1–31. https://doi.org/10.7554/eLife.24634

Ashrafian, H., McKenna, W. J., & Watkins, H. (2011). Disease pathways and novel therapeutic targets in hypertrophic cardiomyopathy. *Circulation Research*, *109*(1), 86–96. https://doi.org/10.1161/CIRCRESAHA.111.242974

Bloemink, M., Deacon, J., Langer, S., Vera, C., Combs, A., Leinwand, L., & Geeves, M. A. (2014). The hypertrophic cardiomyopathy myosin mutation R453C alters ATP binding and hydrolysis of human cardiac β-myosin. *Journal of Biological Chemistry*, *289*(8), 5158–5167. https://doi.org/10.1074/jbc.M113.511204

Colegrave, M., & Peckham, M. (2014). Structural Implications of β-Cardiac Myosin Heavy Chain Mutations in Human Disease. *The Anatomical Record*, *297*(9), 1670–1680. https://doi.org/10.1002/ar.22973

Criddle, A. H., Geeves, M. A., & Jeffries, T. (1985). The use of actin labelled with N-(1-pyrenyl)iodoacetamide to study the interaction of actin with myosin subfragments and troponin/tropomyosin. *Biochemical Journal*, *232*(2), 343 LP-349. Retrieved from http://www.biochemj.org/content/232/2/343.abstract

Cuda, G., Fananapazir, L., Epstein, N. D., & Sellers, J. R. (1997). The in vitro motility activity of beta-cardiac myosin depends on the nature of the beta-myosin heavy chain gene mutation in hypertrophic cardiomyopathy. *Journal of Muscle Research and Cell Motility*, *18*(3), 275–283.

Cuenca, S., Ruiz-Cano, M. J., Gimeno-Blanes, J. R., Jurado, A., Salas, C., Gomez-Diaz, I., … Garcia-Pavia, P. (2016). Genetic basis of familial dilated cardiomyopathy patients undergoing heart transplantation. *Journal of Heart and Lung Transplantation*, *35*(5), 625–635. https://doi.org/10.1016/j.healun.2015.12.014

Deacon, J. C., Bloemink, M. J., Rezavandi, H., Geeves, M. a, & Leinwand, L. a. (2012). Identification of functional differences between recombinant human α and β cardiac myosin motors. *Cellular and Molecular Life Sciences : CMLS*, *69*(13), 2261–77. https://doi.org/10.1007/s00018-012-0927-3

Fananapazir, L., Dalakast, M. C., Cyran, F., Cohn, G., & Epstein, N. D. (1993). Missense mutations in the f8-myosin heavy-chain gene cause central core disease in

hypertrophic cardiomyopathy. *Medical Sciences*, *90*(May), 3993–3997. https://doi.org/10.1073/pnas.90.9.3993

Fenn, W. O. (1923). A quantitative comparison between the energy liberated and the work performed by the isolated sartorius muscle of the frog. *The Journal of Physiology*, *58*(2–3), 175–203. https://doi.org/10.1113/jphysiol.1923.sp002115

García-Giustiniani, D., Arad, M., Ortíz-Genga, M., Barriales-Villa, R., Fernández, X., Rodríguez-García, I., … Monserrat, L. (2015). Phenotype and prognostic correlations of the converter region mutations affecting the β myosin heavy chain. *Heart*, *101*(13), 1047–1053. https://doi.org/10.1136/heartjnl-2014-307205

Geisterfer-Lowrance, A. A. T., Kass, S., Tanigawa, G., Vosberg, H.-P., McKenna, W., Seidman, C. E., & Seidman, J. G. (1990). A molecular basis for familial hypertrophic cardiomyopathy: A β cardiac myosin heavy chain gene missense mutation. *Cell*, *62*(5), 999–1006. https://doi.org/10.1016/0092-8674(90)90274-I

Green, E. M., Wakimoto, H., Anderson, R. L., Evanchik, M. J., Gorham, J. M., Harrison, B. C., … Seidman, C. E. (2016). Heart disease: A small-molecule inhibitor of sarcomere contractility suppresses hypertrophic cardiomyopathy in mice. *Science*, *351*(6273), 617–621. https://doi.org/10.1126/science.aad3456

Greenberg, M. J., Shuman, H., & Ostap, E. M. (2014). Inherent force-dependent properties of β-cardiac myosin contribute to the force-velocity relationship of cardiac muscle. *Biophysical Journal*, *107*(12), L41–L44. https://doi.org/10.1016/j.bpj.2014.11.005

Hamady, M., Buvoli, M., Leinwand, L. A., & Knight, R. (2010). Estimate of the abundance of cardiomyopathic mutations in the β-myosin gene. *International Journal of Cardiology*, *144*(1), 124–126. https://doi.org/10.1016/j.ijcard.2008.12.199

Harris, K. M., Spirito, P., Maron, M. S., Zenovich, A. G., Formisano, F., Lesser, J. R., … Maron, B. J. (2006). Prevalence, clinical profile, and significance of left ventricular remodeling in the end-stage phase of hypertrophic cardiomyopathy. *Circulation*, *114*(3), 216–225. https://doi.org/10.1161/CIRCULATIONAHA.105.583500

Hershberger, R. E., Hedges, D. J., & Morales, A. (2013). Dilated cardiomyopathy: the complexity of a diverse genetic architecture. *Nature Reviews Cardiology*, *10*, 531. Retrieved from http://dx.doi.org/10.1038/nrcardio.2013.105

Homburger, J. R., Green, E. M., Caleshu, C., Sunitha, M. S., Taylor, R. E., Ruppel, K. M., … Ashley, E. A. (2016). Multidimensional structure-function relationships in human β-cardiac myosin from population-scale genetic variation. *Proceedings of the National Academy of Sciences*, *113*(24), 6701–6706. https://doi.org/10.1073/pnas.1606950113

Huang, J., Koide, A., Makabe, K., & Koide, S. (2008). Design of protein function leaps by directed domain interface evolution. *Proceedings of the National Academy of Sciences*, *105*(18), 6578–6583. https://doi.org/10.1073/pnas.0801097105

Huang, J., Nagy, S. S., Koide, A., Rock, R. S., & Koide, S. (2009). A peptide tag system for facile purification and single-molecule immobilization. *Biochemistry*, *48*(50), 11834–11836. https://doi.org/10.1021/bi901756n

Jarcho, J. A., McKenna, W., Pare, J. A., Solomon, S. D., Holcombe, R. F., Dickie, S., … Seidman, C. E. (1989). Mapping a gene for familial hypertrophic cardiomyopathy to chromosome 14q1. *The New England Journal of Medicine*, *321*(20), 1372–1378. https://doi.org/10.1056/NEJM198911163212005

Kaski, J. P., Syrris, P., Esteban, M. T. T., Jenkins, S., Pantazis, A., Deanfield, J. E., … Elliott, P. M. (2009a). Prevalence of sarcomere protein gene mutations in preadolescent children with hypertrophic cardiomyopathy. *Circulation. Cardiovascular Genetics*, *2*(5), 436–41. https://doi.org/10.1161/CIRCGENETICS.108.821314

Kaski, J. P., Syrris, P., Esteban, M. T. T., Jenkins, S., Pantazis, A., Deanfield, J. E., … Elliott, P. M. (2009b). Prevalence of sarcomere protein gene mutations in preadolescent children with hypertrophic cardiomyopathy. *Circulation: Cardiovascular Genetics*, *2*(5), 436–441. https://doi.org/10.1161/CIRCGENETICS.108.821314

Kawana, M., Sarkar, S. S., Sutton, S., Ruppel, K. M., & Spudich, J. (2016). Biophysical properties of human β-cardiac myosin with converter mutations that cause hypertrophic cardiomyopathy, (February), 1–11. https://doi.org/10.1101/065649

Kindel, S. J., Miller, E. M., Gupta, R., Cripe, L. H., Hinton, R. B., Spicer, R. L., … Stephanie, M. (2013). evaluation, *18*(5), 396–403. https://doi.org/10.1016/j.cardfail.2012.01.017.Pediatric

Köhler, J., Winkler, G., Schulte, I., Scholz, T., McKenna, W., Brenner, B., & Kraft, T. (2002). Mutation of the myosin converter domain alters cross-bridge elasticity. *Proceedings of the National Academy of Sciences*, *99*(6), 3557–3562. https://doi.org/10.1073/pnas.062415899

Linari, M., Brunello, E., Reconditi, M., Fusi, L., Caremani, M., Narayanan, T., … Irving, M. (2015). Force generation by skeletal muscle is controlled by mechanosensing in myosin filaments. *Nature*, *528*, 276. Retrieved from https://doi.org/10.1038/nature15727

Lowey, S., Lesko, L. M., Rovner, A. S., Hodges, A. R., White, S. L., Low, R. B., … Robbins, J. (2008). Functional effects of the hypertrophic cardiomyopathy R403Q mutation are different in an α- or β-myosin heavy chain backbone. *Journal of Biological Chemistry*, *283*(29), 20579–20589. https://doi.org/10.1074/jbc.M800554200

Mijailovich, S. M., Li, X., del Álamo, J. C., Griffiths, R. H., Kecman, V., & Geeves, M. A. (2010). Resolution and uniqueness of estimated parameters of a model of thin filament regulation in solution. *Computational Biology and Chemistry*, *34*(1), 19–33. https://doi.org/10.1016/j.compbiolchem.2009.11.002

Mijailovich, S. M., Nedic, D., Svicevic, M., Stojanovic, B., Walklate, J., Ujfalusi, Z., & Geeves, M. A. (2017). Modeling the Actin.myosin ATPase Cross-Bridge Cycle for Skeletal and Cardiac Muscle Myosin Isoforms. *Biophysical Journal*, *112*(5), 984–996. https://doi.org/10.1016/j.bpj.2017.01.021

Mohamed, A. S., Dignam, J. D., & Schlender, K. K. (1998). Cardiac myosin-binding

protein C (MyBP-C): identification of protein kinase A and protein kinase C phosphorylation sites. *Archives of Biochemistry and Biophysics*, *358*(2), 313–319. https://doi.org/10.1006/abbi.1998.0857

Mohiddin, S. A., Begley, D. A., McLam, E., Cardoso, J.-P., Winkler, J. B., Sellers, J. R., & Fananapazir, L. (2003). Utility of genetic screening in hypertrophic cardiomyopathy: prevalence and significance of novel and double (homozygous and heterozygous) beta-myosin mutations. *Genetic Testing*, *7*(1), 21–27. https://doi.org/10.1089/109065703321560895

Morita, H., Rehm, H. L., Menesses, A., McDonough, B., Roberts, A. E., Kucherlapati, R., … Seidman, C. E. (2008). Shared genetic causes of cardiac hypertrophy in children and adults. *The New England Journal of Medicine*, *358*(18), 1899–908. https://doi.org/10.1056/NEJMoa075463

Nag, S., Sommese, R. F., Ujfalusi, Z., Combs, A., Langer, S., Sutton, S., … Spudich, J. A. (2015). Contractility parameters of human beta-cardiac myosin with the hypertrophic cardiomyopathy mutation R403Q show loss of motor function. *Science Advances*, *1*(9), e1500511. https://doi.org/10.1126/sciadv.1500511

Neubauer, S. (2007). The Failing Heart — An Engine Out of Fuel. *The New England Journal of Medicine*, *356*, 1140–1151. https://doi.org/10.1056/NEJMra063052

Palmer, B. M., Fishbaugher, D. E., Schmitt, J. P., Wang, Y., Alpert, N. R., Seidman, C. E., … Maughan, D. W. (2004). Differential cross-bridge kinetics of FHC myosin mutations R403Q and R453C in heterozygous mouse myocardium. *American Journal of Physiology, Heart and Circulatory*, *287*(1), H91-9. https://doi.org/10.1152/ajpheart.01015.2003

Previs, M. J., Mun, J. Y., Michalek, A. J., Previs, S. B., Gulick, J., Robbins, J., … Craig, R. (2016). Phosphorylation and calcium antagonistically tune myosin-binding protein C's structure and function. *Proceedings of the National Academy of Sciences*, *113*(12), 3239–3244. https://doi.org/10.1073/pnas.1522236113

Resnicow, D. I., Deacon, J. C., Warrick, H. M., Spudich, J. a, & Leinwand, L. a. (2010). Functional diversity among a family of human skeletal muscle myosin motors. *Proceedings of the National Academy of Sciences of the United States of America*, *107*(3), 1053–8. https://doi.org/10.1073/pnas.0913527107

Robert-Paganin, J., Auguin, D., & Houdusse, A. (2018). Hypertrophic cardiomyopathy disease results from disparate impairments of cardiac myosin function and auto-inhibition. *Nature Communications*, *9*(1). https://doi.org/10.1038/s41467-018-06191-4

Seebohm, B., Matinmehr, F., Köhler, J., Francino, A., Navarro-Lopéz, F., Perrot, A., … Kraft, T. (2009). Cardiomyopathy mutations reveal variable region of myosin converter as major element of cross-bridge compliance. *Biophysical Journal*, *97*(3), 806–824. https://doi.org/10.1016/j.bpj.2009.05.023

Smith, D. A. (2014). A new mechanokinetic model for muscle contraction, where force and movement are triggered by phosphate release. *Journal of Muscle Research and Cell Motility*, *35*(5–6), 295–306. https://doi.org/10.1007/s10974-014-9391-z

Smith, D. A., & Geeves, M. A. (1995). Strain-dependent cross-bridge cycle for muscle. II. Steady-state behavior. *Biophysical Journal*, *69*(2), 538–552. https://doi.org/10.1016/S0006-3495(95)79927-1

Sommese, R. F., Sung, J., Nag, S., Sutton, S., Deacon, J. C., Choe, E., … Spudich, J. A. (2013). Molecular consequences of the R453C hypertrophic cardiomyopathy mutation on human -cardiac myosin motor function. *Proceedings of the National Academy of Sciences*, *110*(31), 12607–12612. https://doi.org/10.1073/pnas.1309493110

Spudich, J. A. (2015). The myosin mesa and a possible unifying hypothesis for the molecular basis of human hypertrophic cardiomyopathy. *Biochemical Society Transactions*, *43*(1), 64–72. https://doi.org/10.1042/BST20140324

Spudich, J. a., & Watt, S. (1971). The Regulation of Rabbit Skeletal Muscle Contraction. *The Journal of Biological Chemistry*, *245*(15), 4866–4871.

Stewart, B. S., Mason, D. T., & Braunwald, E. (1968). Impaired Rate, *XXXVII*(January), 8–15.

Teekakirikul, P., Kelly, M. A., Rehm, H. L., Lakdawala, N. K., & Funke, B. H. (2013). Inherited cardiomyopathies: molecular genetics and clinical genetic testing in the postgenomic era. *The Journal of Molecular Diagnostics : JMD*, *15*(2), 158–170. https://doi.org/10.1016/j.jmoldx.2012.09.002

Toepfer, C., Caorsi, V., Kampourakis, T., Sikkel, M. B., West, T. G., Leung, M. C., … Ferenczi, M. A. (2013). Myosin regulatory light chain (RLC) phosphorylation change as a modulator of cardiac muscle contraction in disease. *Journal of Biological Chemistry*, *288*(19), 13446–13454. https://doi.org/10.1074/jbc.M113.455444

Trivedi, D. V., Adhikari, A. S., Sarkar, S. S., Ruppel, K. M., & Spudich, J. A. (2017). Hypertrophic cardiomyopathy and the myosin mesa: viewing an old disease in a new light. *Biophysical Reviews*, (Huxley 1957). https://doi.org/10.1007/s12551-017-0274-6

Tyska, M. J., Hayes, E., Giewat, M., Seidman, C. E., Seidman, J. G., & Warshaw, D. M. (2000). Single-Molecule Mechanics of R403Q Cardiac Myosin Isolated From the Mouse Model of Familial Hypertrophic Cardiomyopathy.

Ujfalusi, Z., Vera, C. D., Mijailovich, S. M., Svicevic, M., Yu, E. C., Kawana, M., … Leinwand, L. A. (2018). Dilated cardiomyopathy myosin mutants have reduced force-generating capacity. *Journal of Biological Chemistry*, (Dcm), jbc.RA118.001938. https://doi.org/10.1074/jbc.RA118.001938

Walklate, J., Vera, C., Bloemink, M. J., Geeves, M. A., & Leinwand, L. (2016). The most prevalent freeman-sheldon syndrome mutations in the embryonic myosin motor share functional defects. *Journal of Biological Chemistry*, *291*(19), 10318–10331. https://doi.org/10.1074/jbc.M115.707489

Zot, H. G., & Potter, J. D. (1981). Purification of Actin from Cardiac Muscle. *Preparative Biochemistry*, *11*(4), 381–395. https://doi.org/10.1080/00327488108065530

Methods

Expression and purification of proteins – Producing recombinant β-cardiac myosin in C2C12 cells in several iterations, isoforms, and mutants has been described previously in (Bloemink et al., 2014; Deacon et al., 2012; Nag et al., 2015; Resnicow, Deacon, Warrick, Spudich, & Leinwand, 2010; Ujfalusi et al., 2018; Walklate, Vera, Bloemink, Geeves, & Leinwand, 2016). The sS1 (residues 1-808) was followed by a flexible GSG (Gly-Ser-Gly) linker and a C-terminal 8-residue (RGSIDTWV) PDZ-binding peptide. Human ventricular essential light chain (MYL3 or ELC) with either a 6X-His or a FLAG tag was co-expressed with the heavy chain. Over the course of the different experiments a combination of affinity and ionic exchange chromatography were used as in our previous studies (i.e. His or FLAG + Q column). The fast kinetics experiments in this study were done with protein purified with double affinity, a His-NTA resin and the PDZ-C-tag affinity system described in (Jin Huang, Nagy, Koide, Rock, & Koide, 2009). WT-erbin PDZ was prepared as described in (Huang et al. 2008, 2009) and crosslinked to the Sulfolink Coupling Resin (Thermo Fisher) using the manufacturer's protocol. After the myosin was eluted from the His column, the sample was dialyzed into 1X TBS to remove the imidazole from the His column. The PDZ system uses 20-50 μM of "elution peptide" (NH_2-WETWV-COOH from GenScript). After the second column, the myosin samples were buffer exchanged and frozen in the proper assay buffer. Actin preparations were made from bovine left ventricle with protocols adapted from (J. a. Spudich & Watt, 1971; Zot & Potter, 1981). The protocol for preparing pyrene-labelled actin is based on the methods described in (Criddle, Geeves, & Jeffries, 1985).

Steady-state actin-activated ATPase assays – All ATPase experiments were performed at 23 °C room temperature in a buffer containing 10 mM imidazole, 3 mM $MgCl_2$, 5 mM KCl, and 1 mM DTT at pH 7.5. A colorimetric assay to measure inorganic phosphate production at various time points and actin concentrations ranging 0 – 100 µM. The rates of phosphate production were plotted and fitted to the Michaelis-Menten equation using Origin (OriginPro) and/or GraphPad Prism to obtain the k_{cat} and K_m.

Transient kinetics – All stopped-flow measurements were performed at 20°C in 20 mM MOPS, 25 mM KCl, 5 mM $MgCl_2$, 1 mM NaN_3 at pH 7.0, unless indicated otherwise. Rapid-mixing experiments using 2-5 biological replicates, with 4-6 technical replicates, over a wide range of experimental substrates were performed in a High-Tec Scientific SF-61 DX2 stopped-flow system. Transient kinetic traces were initially fitted with TgK Scientific (Kinetic Studios) and subsequently plotted with Origin (OriginPro). For experiments probing the actin-myosin interaction with ATP and ADP we utilized the fluorescence signal for the pyrene-labelled actin, which has an excitation wavelength at 365-nm and the emission was detected after passing through KV389-nm cut-off filter. In the absence of actin, we relied on the intrinsic tryptophan fluorescence post-nucleotide binding where a tryptophan on the relay helix can be excited at 295-nm and the emission is detected with WG-320 filter.

Modelling analysis - The parameters estimated experimentally by the transient kinetics analysis can be utilized to model the cross-bridge cycle by having a good estimate of the k_{cat} and K_m values obtained from the ATPase experiments and using the in-house MUSICO software (Srbolujub M. Mijailovich et al., 2017). We previously reported a kinetic modeling analysis of five DCM mutations using this approach (Ujfalusi et al., 2018). This

can be employed to predict the transient occupancy of the states in the myosin ATPase cycle, across a wide range of actin concentrations assuming initially a state where [ADP] = [P_i] = 0, and the system proceeds to steady-state activity (Srbolujub M. Mijailovich et al., 2017). The different steps of the cycle have interdependence to each other, thus to properly fit the rate and equilibrium constants of the cycle, it is important that the experimental data provide a uniquely resolved set of modelling parameters (Fig 5.4) (Srboljub M Mijailovich et al., 2010). Consistent with our previous modeling work, the fitted parameters are defined to a precision of ~20%. Other well-defined assumptions and estimates applied to this mechano-chemical cycle model for β-MyHC are the isoform-specific constraint effect and the effect of load on the motor (Greenberg, Shuman, & Ostap, 2014; D. A. Smith & Geeves, 1995). For a muscle fiber under isometric tension an approximate 5 pN of load with a 3-fold reduction in the ADP release rate constant are suggested as good estimates. This reduction of the ADP-release rate has little-effect on the ATP flux, because this step is significantly faster than the overall k_{cat}. Additionally, the rate of entry into the force-generating state is expected to be inhibited by load via the Fenn effect (Fenn, 1923). Therefore, a 3-fold inhibition of the ATPase flux by reducing the entry into the force-holding state (A·M·D) which is k_{Pi} in our model (David A. Smith, 2014). This assumes that a load will impact the P_i and ADP release steps similarly.

In vitro motility - All the experiments were performed at 23°C. Glass coverslips (VWR micro cover glass) were coated with a mixture of 0.2% nitrocellulose (Ernest Fullam Inc.) and 0.2% collodion (Electron Microscopy Sciences) dissolved in amyl acetate (Sigma) and air-dried before use. A permanent double-sided tape (Scotch) was used to construct four channels in each slide, and four different experiments were performed on the same

slide. Partially inactivated myosin heads in S1 preparations were removed by the 'dead-heading' process before performing the motility assay. The process of 'dead-heading' had the following steps: A ten-fold molar excess of F-actin was added to myosin in the presence of 2 mM ATP; the mixture was incubated for 15 min in an ice bucket; 50 mM MgCl2 was added to form F-actin Mg^{2+}-paracrystals and incubated for 5 min; the paracrystals were sedimented at 350,000g for 15 min; supernatant was collected, and the sS1concentration was measured using the Bradford reagent (Bio-Rad). Before any experiments, dead-headed sS1 was diluted in 10% ABBSA [assay buffer (AB; 25 mM imidazole, pH 7.5, 25 mM KCl, 4 mM $MgCl_2$, 1 mM EGTA, and 1 mM DTT) with bovine serum albumin (BSA, 0.1 mg/ml) diluted in AB], unless otherwise stated.

For motility experiments using pure actin, reagents were sequentially flowed through the channels in the following order: 10 µl of 4 µM SNAP-PDZ18 diluted in AB and incubated for 3 min; 20 ul of ABBSA to block the surface from nonspecific attachments and incubated for 2 min; 10 µl of a mixture of eight-residue (RGSIDTWV)-tagged human ß-cardiac sS1 (~0.05 to 0.1 mg/ml) and incubated for 3 min; 20 µl of AB to wash any unattached proteins; and finally, 10 µl of the GO solution [5 to 10 nM tetramethylrhodamine (TMR)-phalloidin (Invitrogen)- labeled bovine actin, 2 mM ATP (Calbiochem), an oxygen-scavenging system consisting of 0.2% glucose, glucose oxidase (0.11 mg/ml; Calbiochem), and catalase (0.018 mg/ml; Calbiochem)], and an ATP regeneration system consisting of 1 mM phosphocreatine (Calbiochem) and creatine phosphokinase (0.1 mg/ml; Calbiochem) in ABBSA].

ACKNOWLEDGEMENTS: J.A.S. is a co-founder of Cytokinetics and MyoKardia. L.A.L. is a co-founder of MyoKardia. J.A.S., L.A.L., and K.M.R. are members of the scientific advisory board for MyoKardia. The authors are supported by the following funding sources: Children's Cardiomyopathy Foundation (L.A.L), National Institutes of Health 2R01GM029090 (M.A.G., L.A.L., C.D.V), National Institutes of Health 3R01GM029090-31S1 (C.D.V.), National Institutes of Health 1F31GM111058-01A1 (C.D.V) and National Institutes of Health 2R01HL117138-05 (L.A.L., J.A.S., C.D.V.). M.A.G. & J.W. received funding from the European Union's Horizon 2020 Research and Innovation Programme grant No. 777204 SILICOFCM. We also thank Sam Lynn for technical assistance

AUTHOR CONTRIBUTIONS: M.A.G. and L.A.L. conceived the study and supervised each step of the work. C.D.V. designed, performed and analyzed steady-state and pre-steady state experiments, and responsible for cell culture, adenovirus and protein preparations. C.A.J. with J.W. and Z.U. designed and performed stopped-flow experiments as well as initiating most of the kinetic modeling analysis. C.A.J., Z.U., S.M.M., and M.S. completed the kinetic modeling. A.C. and S.J.L. provided substantial technical support in cell culture. A.S.A., K.M.R., and J.A.S. designed and performed ATPase, *in vitro* motility assays and the respective data analysis.

	β-WT		Pediatric				Adult		
		H251N	D382Y	F540L	P710R	V763M	R719W	R723G	G741R
ATP binding to sS1									
Second order rate constant of ATP binding ($\mu M^{-1}s^{-1}$)	**5.8 ± 0.4**	6.4 ± 0.6	3.3 ± 0.6	2.9 ± 0.3	0.6 ± 0.07	3.1 ± 0.9	5.3 ± 1.7	4.1 ± 0.3	3.4 ± 0.7
$K_{50\%}$ (μM)	**15.9 ± 2.2**	20.3 ± 3.4	27.6 ± 4.1	20.9 ± 2.8	35.7 ± 0.9	20.9 ± 3.2	14.1 ± 4.8	21.3 ± 2.5	37.8 ± 14.2
k_H+k_{-H} (s^{-1})	**91.2 ± 1.8**	125.7 ± 9.3	88.6 ± 2.0	59.2 ± 4.85	69.1 ± 7.1	63.3 ± 8.6	58.2 ± 3.5	86.5 ± 4.2	106.5 ± 15.6
ADP binding to sS1									
ADP affinity (μM)	**0.53 ± 0.06**	0.19 ± 0.01	0.220 ± 0.034	0.180 ± 0.035	3.1 ± 1.0	0.312	0.241	0.259	0.18 ± 0.03
Rate constant of ADP release (s^{-1})	**0.63 ± 0.03**	1.0 ± 0.2	0.51 ± 0.06	0.4 ± 0.0	0.14 ± 0.005	1.2	0.9 ± 0	0.98	0.71 ± 0.02
ATP binding to acto.sS1									
$K_T k_{+T'}$ ($\mu M^{-1}s^{-1}$) 20°C	**4.4 ± 0.3**	5.1 ± 0.4	4.5 ± 0	3.6 ± 0.2	7.1 ± 0.7	4.4 ± 0.5	6.0 ± 1.0	5.0 ± 0.5	4.9 ± 0.8
K_T (μM) 20°C	**327.9 ± 53.3**	131 ± 19	289.7 ± 65.3		161.0 ± 18.3	270.0 ± 78.8	125.6 ± 75.3	202.9 ± 60.4	178.4 ± 11.8
$k_{+T'}$ (s^{-1}) 20°C	**1543 ± 100**	666 ± 58	1300.7 ± 297.1	1897	1106.5 ± 73.2	1175.8 ± 283.0	676 ± 145.9	556.1 ± 235.2	940.3 ± 336
$K_T k_{-T'}$ ($\mu M^{-1}s^{-1}$) 10°C	**2.7 ± 0.09**	3.2	3.1 ± 0.2	2.1 ± 0.15	3.9 ± 0.9	3.3 ± 0.5	3.2 ± 0.3	2.9 ± 0.2	2.7 ± 0.2
K_T (μM) 10°C	**365.7 ± 17.7**	187	239.5 ± 21.1	526.9 ± 39.1	251.5 ± 108.9	214.0 ± 23.3	184.9 ± 25.5	211.4 ± 41.0	224.0 ± 22.9
$k_{+T'}$ (s^{-1}) 10°C	**991 ± 18.2**	592	741.2 ± 28.4	1098.9 ± 20.8	814.1 ± 134.7	699.6 ± 62.5	573.2 ± 25.3	638.6 ± 56.0	639.8 ± 68.4
ADP affinity for acto.sS1									
$((K_{D'}+1)/K_D K_{D'})$ (μM)	**6.1 ± 0.7**	20.8 ± 3.6	17.6 ± 2.7	7.9 ± 0.5	14.6 ± 3.0	18.6 ± 8.4	15.9 ± 2.7	6.5 ± 0.7	10.1 ± 3.0
$k_{+D'}$ (s^{-1})	**58.7 ± 3.3**	56.7 ± 2.9	64.3 ± 2.4	54.8 ± 4.1	69.1 ± 0.6	68.1 ± 10.5	96.8 ± 0.5	106.8 ± 0.3	71.1 ± 4.8
$K_D k_{-D'}$ ($\mu M^{-1}s^{-1}$)	**9.6**	2.7	3.7	6.9	4.7	3.8	5.9	16.4	7.0
sS1 affinity for actin									
K_A (nM)	**10 ± 1.8**	8.7 ± 1.5	4.6	2.3 ± 0.1	<10	6.5 ± 3.8	1.6 ± 0.1	13.6	8.7 ± 4.7
K_{DA} (nM)	**109.3 ± 13.8**	56.3 ± 9.3		5.2 ± 0.5	12.2 ± 6.3	24.6	35 ± 8.2	48.4	23.1
K_{DA}/K_A	**10.9**	6.5		2.3	1.2	4.1	21.9	3.6	2.7
ATPase									
k_{cat} (s^{-1})	**4.5 ± 0.4***	5.6 ± 0.4**	4.3 ± 0.3#	6.4 ± 0.3#	2.8 ± 0.2#	4.5 ± 0.4#	5.4 ± 0.4***	3.2 ± 0.2***	4.6 ± 0.3***
K_{app} (μM)	**58 ± 9***	60 ± 10**	64 ± 10#	31 ± 5#	24 ± 5#	27 ± 5#	34 ± 4***	30 ± 4***	23 ± 3***
k_{cat}/K_{app} ($s^{-1}\mu M^{-1}$)	**0.078**	0.093	0.067	0.206	0.117	0.167	0.159	0.107	0.20

No (significant) change from WT
>30% slower/weaker
>2 fold slower/weaker
>30% faster/tighter
>2 fold faster/stronger

Table 1. Kinetic parameters for β-WT and 8 HCM mutations. The color code described in the smaller table to the right indicates degree of difference from WT. Experimental conditions for stopped-flow: 25 mM KCl, 5 mM $MgCl_2$, 20 mM MOPS, pH 7.0, 20 °C. Data are the mean ± S.E. values from 3-5 independent measurements with 4-6 technical replicates. Bottom of the table contains the ATPase values used for modeling:

*****ATPase values from Adhikari *et al*.

******ATPase values from Kawana *et al*.

*******Unpublished ATPase values.

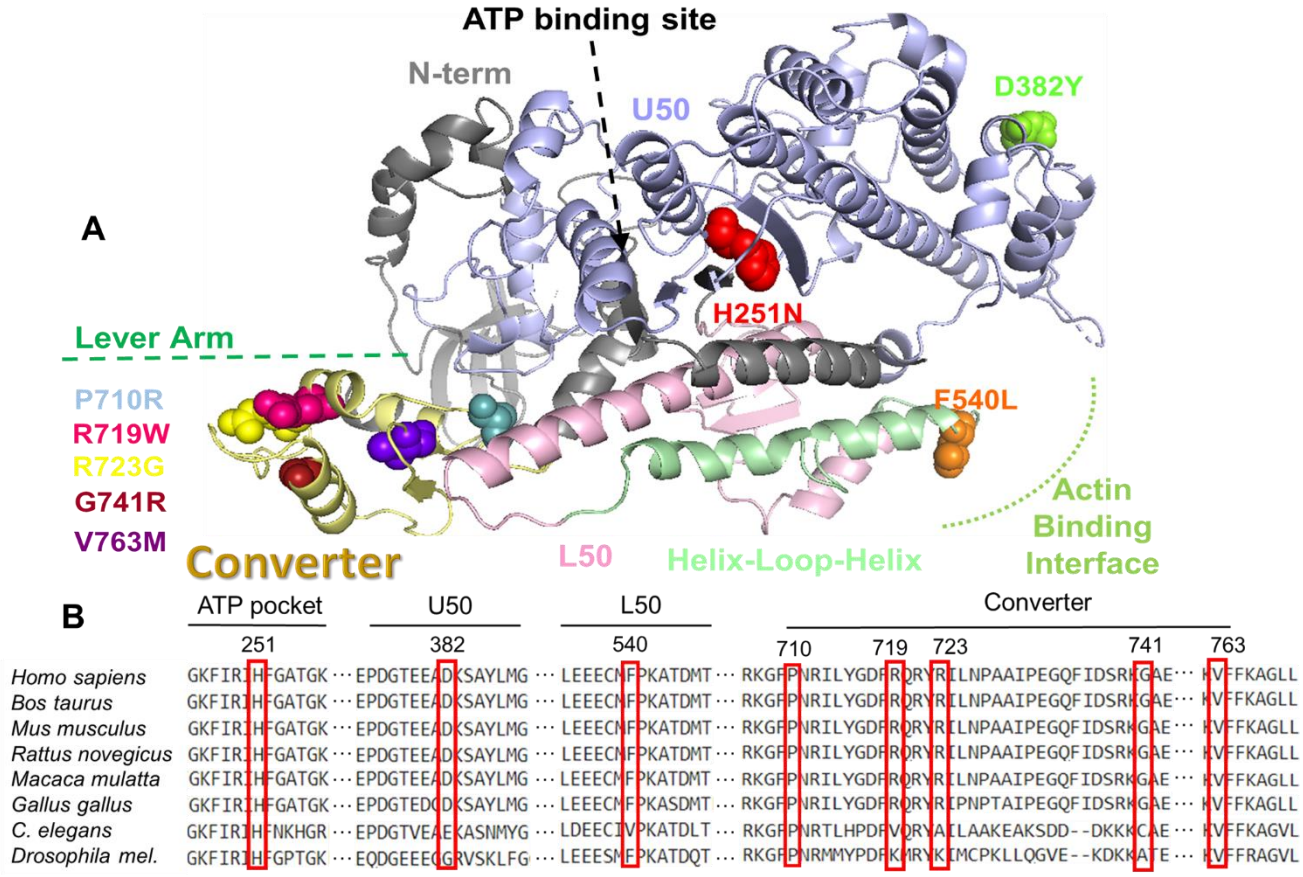

Figure 1. Structural location of HCM mutations. (A) Structural model of the catalytic domain of *β-MyHC* (based on PDB 4P7H). The heavy chain is shown as a ribbon diagram with the major subdomains and HCM mutations color-coded for the reader. The mutations sites are shown in space filling form in individual colors. The same colors are used throughout the figures and tables. Color code: Red-H251N; Green-D382Y; Orange-F540L; Light blue-P710R; Purple-V763M; Pink-R719W; Yellow-R723G; Maroon-G741R. (B) Alignment of conserved *MYH7* residues where mutations discussed throughout this study can be found.

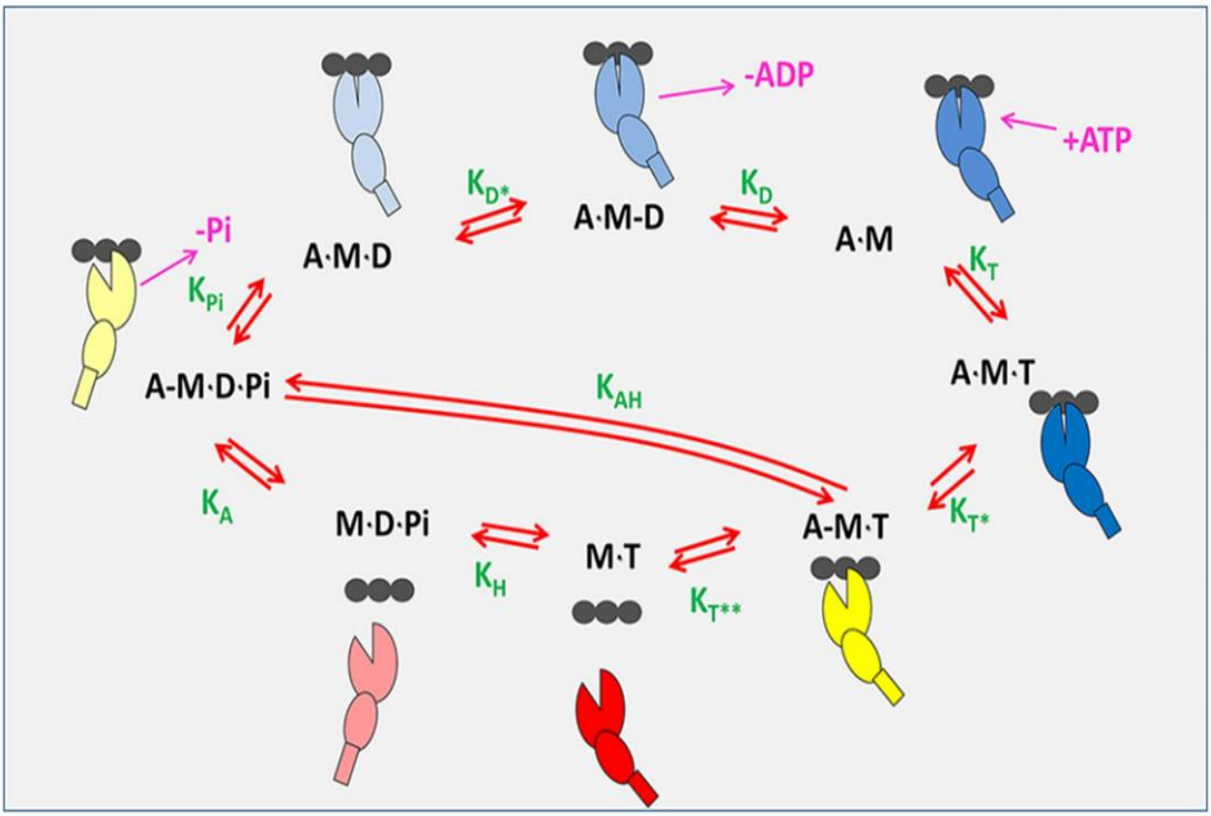

Figure 2. Actin·myosin ATPase-driven cross-bridge cycle. As discussed in (Mijailovich et al 2017) the basic ATPase cycle for myosin can be described in 8 steps: ATP binding to acto.myosin, ATP-induced conformational change that weakens actin affinity, ATP-induced dissociation from actin, ATP hydrolysis, actin re-attachment, P_i-release + power stroke, conformational change in the transducer region coordinating ADP for release, and ending with ADP release. The myosin is a composite of a large ellipse (motor domain), a smaller ellipse (converter), and a small rectangle (lever arm) binding to an actin filament depicted as three black ellipses. A blue-shaded myosin is strongly-attached to actin (closed ellipse) and is progressively darker as it approaches the rigor state. The myosins with an open cleft are shown in yellow (weakly-attached) and red (detached). Nucleotide and P_i release are show in cerise. Equilibrium constants for each step are shown in green and defined in the clockwise direction.

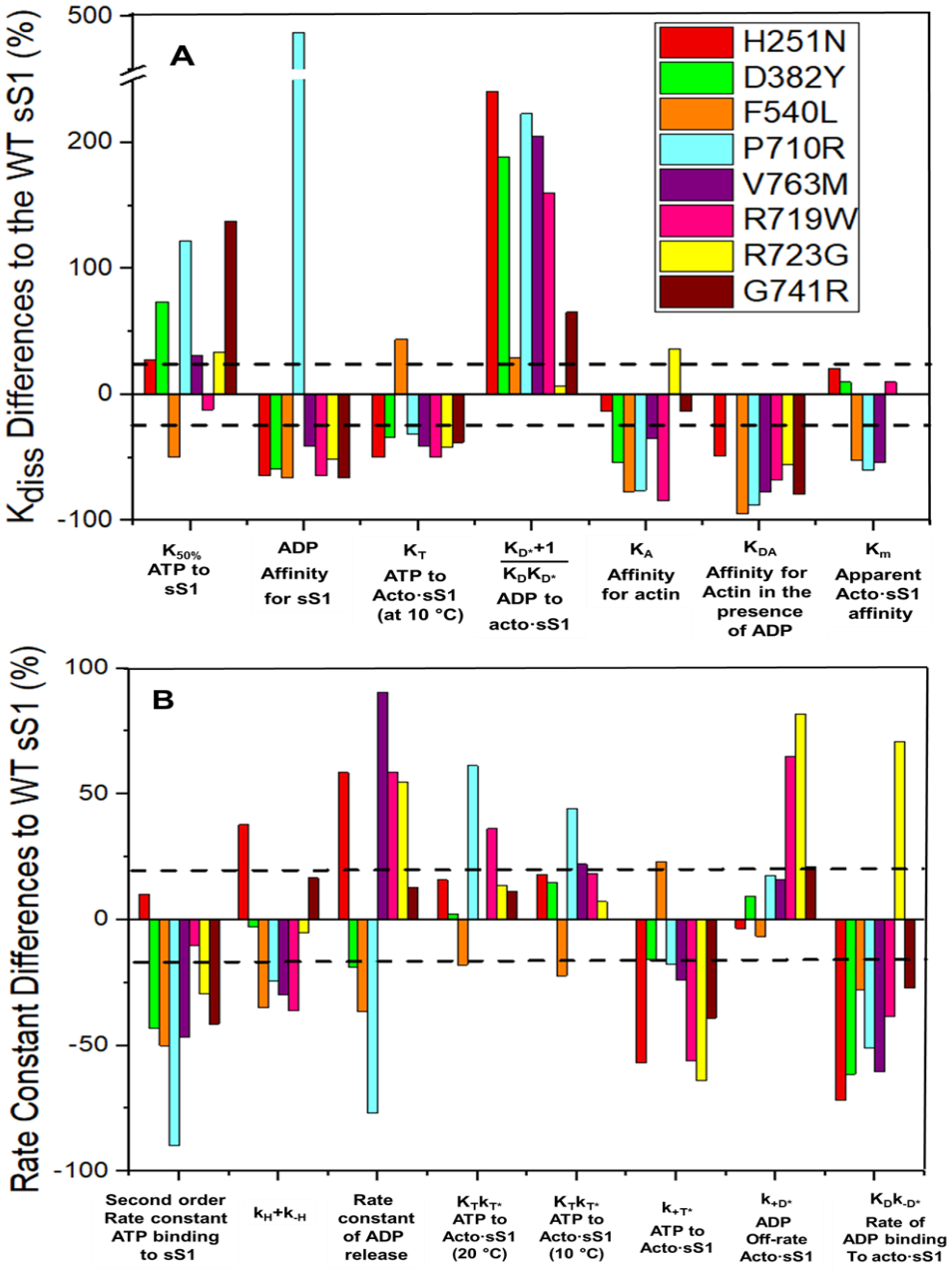

Figure 3. Summary of percentage differences in kinetic parameters of HCM mutations relative to WT. (A) %-change for measured dissociation or equilibrium constants. Also included is the apparent K_m from ATPase analysis. (B) %-change of several measured rate constants. Color-coded to match the parameter to each HCM mutation. The dashed line represents 20% change in the parameter considered to be the precision of each measurement.

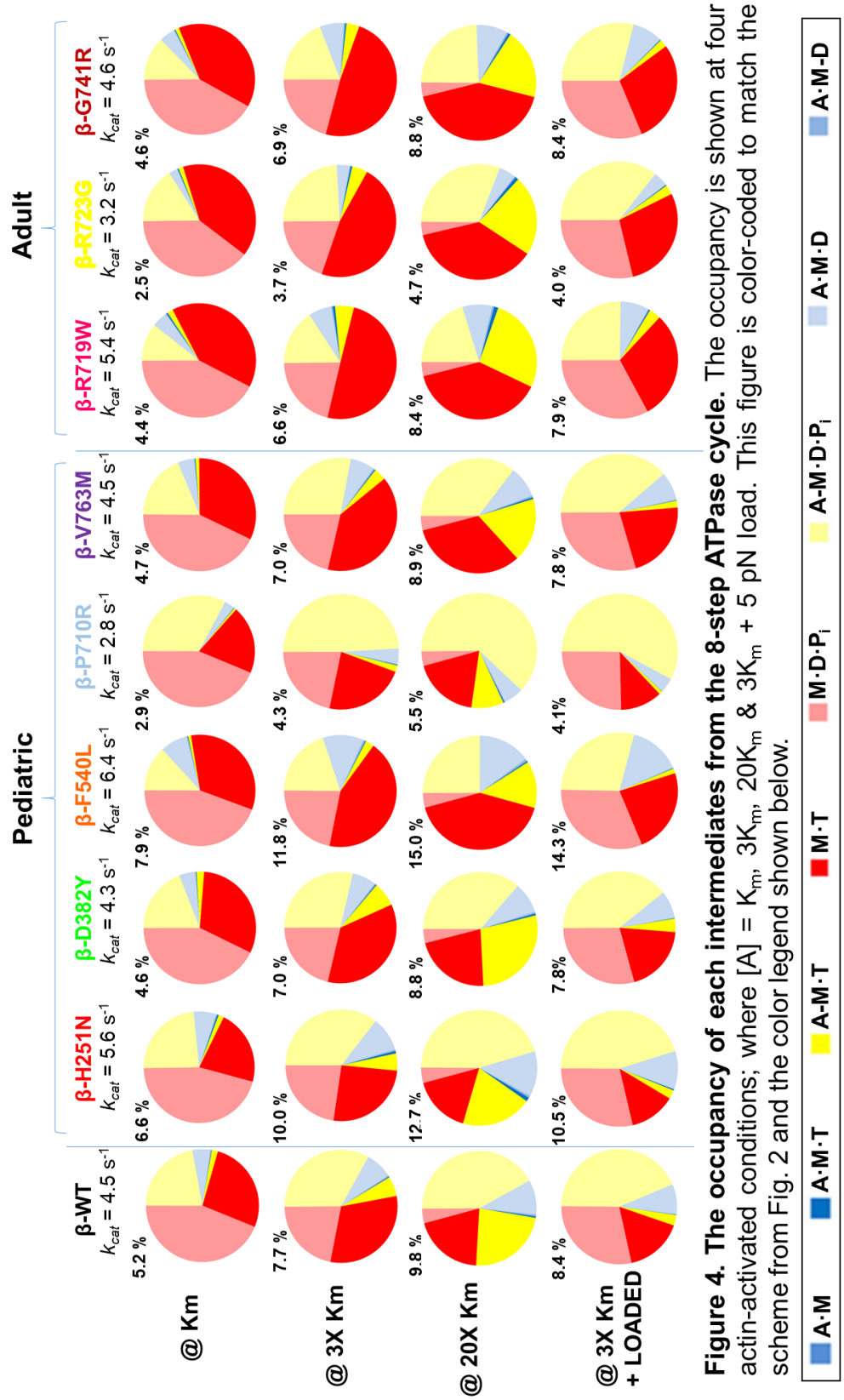

Figure 4. The occupancy of each intermediates from the 8-step ATPase cycle. The occupancy is shown at four actin-activated conditions; where [A] = K_m, 3K_m, 20K_m & 3K_m + 5 pN load. This figure is color-coded to match the scheme from Fig. 2 and the color legend shown below.

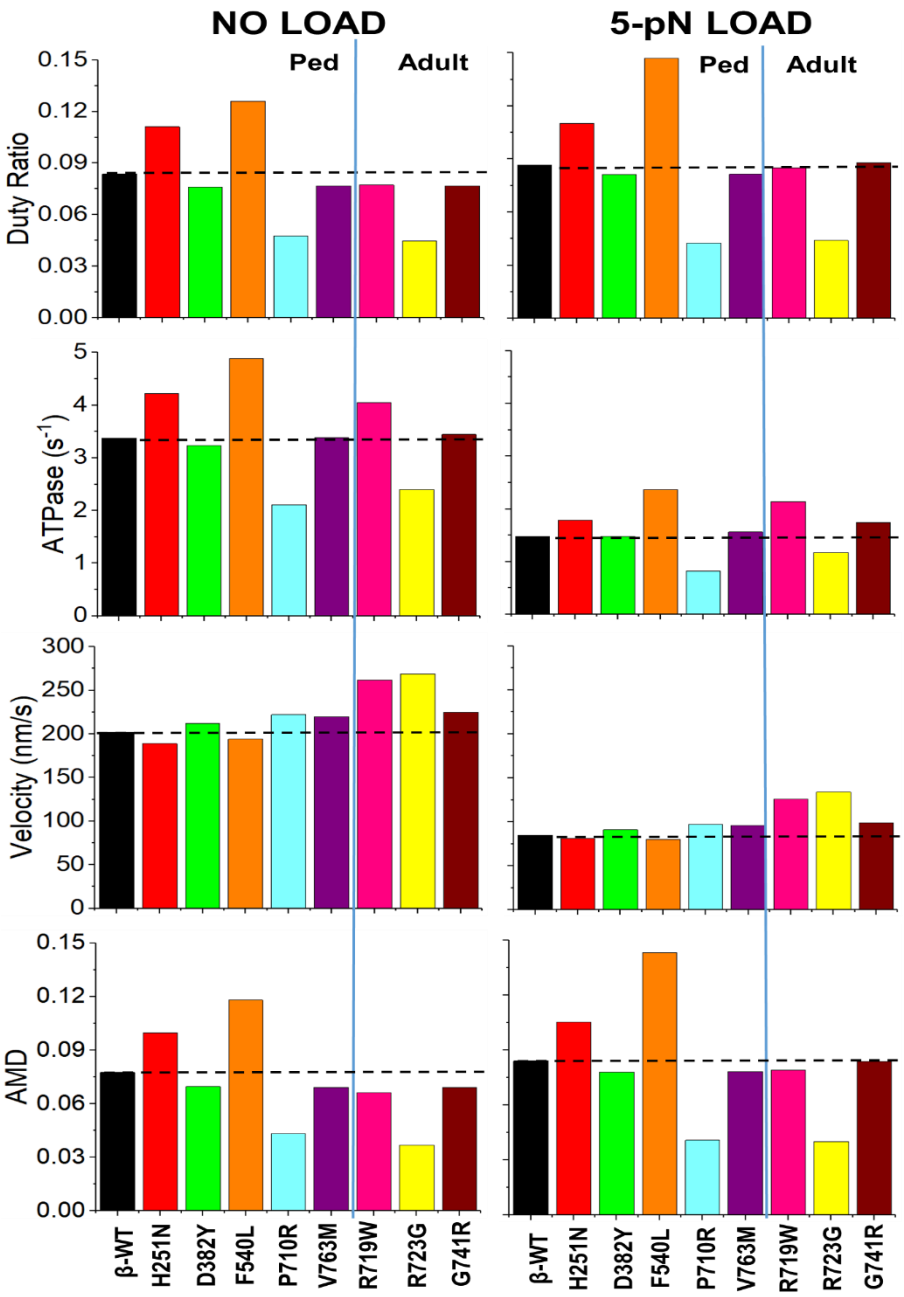

Figure 5. The calculated values for duty ratio, *ATPase*, maximum shortening velocity, and occupancy of the force-holding A·M·D state for each of the HCM-causing mutations studied. The dashed line indicates the WT protein value. The left bar charts show the values based on kinetic measurements at [A] = 3 K_m. The right bar charts are the predicted results if the myosin additionally bears a 5-pN load.

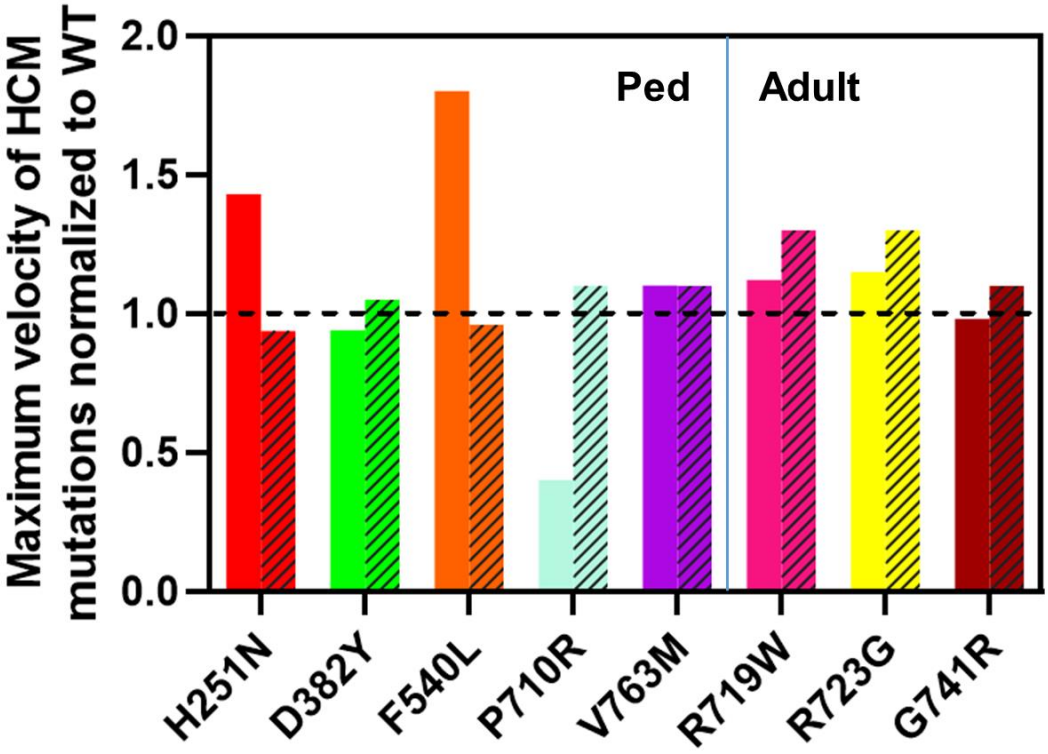

Figure 6. Comparison of normalized *in vitro* motility values to the predicted velocity of shortening. The solid coloring depicts the top 5% mean velocity values measured experimentally through unloaded *in vitro* motility. The bars with hatched patterns are the values predicted for the kinetic model analysis as described in (Ujfalusi et al 2018). The dashed line indicates the normalized WT value of 1 for comparing the mutations.

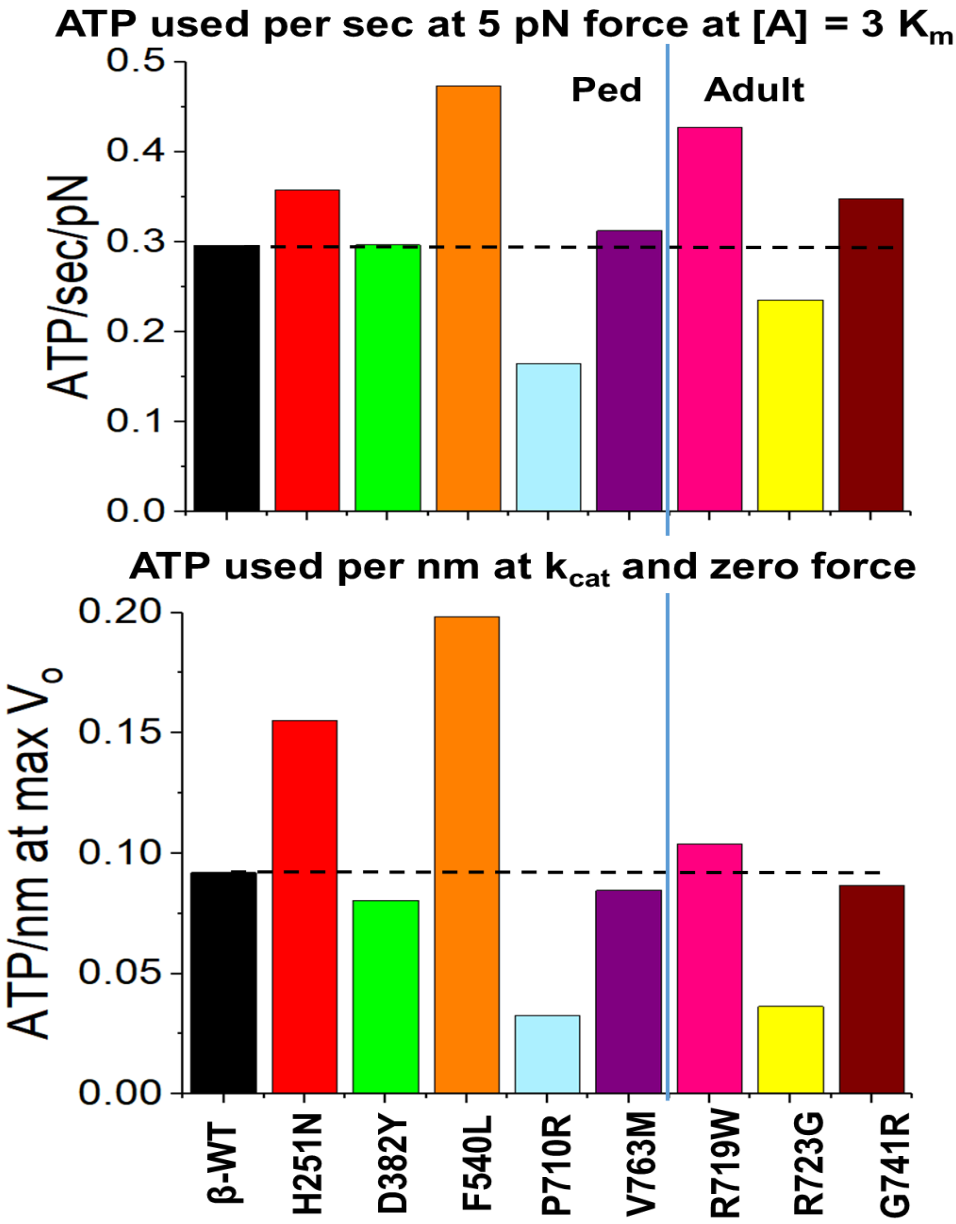

Figure 7. Economy of force generation and velocity for HCM mutations. Top, ATP usage per second per pN of force while generating 5 pN of force at [A] = 3 K_m, Bottom, ATP used per second at maximum shortening velocity (zero load). Because ATPase and DR have the same dependence on [A], this calculation is the same at all actin concentrations except very low values where the motor cannot maintain constant velocity.